

## Stochastic and Adiabatic Behavior of Particles Accelerated by Periodic Forces\*

M. A. Lieberman and A. J. Lichtenberg

*Department of Electrical Engineering and Computer Sciences and the Electronics Research Laboratory,  
University of California, Berkeley, California 94720*

(Received 13 May 1971)

The mechanism by which periodic nonrandom forces lead to stochastic acceleration of particles is examined. Two examples considered are (i) the Fermi problem of a ball bouncing between a fixed and an oscillating wall, with various wall-oscillation functions, and (ii) cyclotron-resonance heating in a magnetic mirror. Numerical studies show that the phase plane consists of a complicated but regular structure of islands embedded in a stochastic sea. These islands may have the character of either adiabatic barriers or sinks for particles. The islands can be described analytically by expansions about elliptic singular points. A velocity below which no islands exist is observed computationally and is predicted from Floquet theory. Computations also demonstrate that in some cases an adiabatic wall forms an upper limit to particle diffusion in velocity space. A lower bound on this wall is predicted analytically. The Fermi problem is reduced to a Hamiltonian form, and the nonlinear stability and approximate location of the adiabatic wall is predicted from adiabatic invariance theory. Introduction of an external random-force component modifies, but does not destroy, the basic results. For velocities below which no islands exist, it is shown that the random-phase assumption holds, and that the particle motion can be described by a Fokker-Planck equation. The solution to the Fokker-Planck equation is found to agree with the numerical calculations. Above the stochastic transition velocity, strong phase correlations exist, and a Fokker-Planck description is inappropriate.

### I. INTRODUCTION

It is well known<sup>1-4</sup> that in a large class of problems having more than one degree of freedom there are parameter ranges for which adiabatic invariants exist that separate the degrees of freedom. The phase space for each degree then exhibits adiabatic behavior; i.e., the trajectory of the solution is a closed curve in the phase plane. For other parameter ranges, one or more of the invariants may not exist, such that the trajectory in a single phase plane is area filling. Similar behavior is found for one-dimensional nonlinear oscillators with periodic coefficients. Results of the adiabatic theory and the numerical computations are summarized in Ref. 4.

A one-dimensional acceleration problem fitting into the above scheme that has received considerable attention is that of a ball bouncing between a fixed and an oscillating wall. The problem was first examined by Fermi<sup>5</sup> as an analog to a possible cosmic-ray acceleration mechanism, and will be referred to here as the Fermi acceleration problem. Early numerical calculations by Fermi<sup>5</sup> and others<sup>6,7</sup> gave conflicting results, sometimes indicating oscillatory energy changes of the ball,<sup>6</sup> and sometimes indicating that the momentum transfer was stochastic, i.e., that the ball struck the oscillatory wall with a random phase with respect to the wall oscillation.<sup>7</sup> Zaslavskii and Chirikov<sup>8</sup> partially resolved this contradiction by demonstrating that for high ball velocities, such that the

transit time of the ball was comparable to the wall-oscillation period, an adiabatic invariant existed which limited the energy excursions. For lower velocities, they postulated that similar invariants did not exist, and made numerical computations which they interpreted as verifying their assumption.

As is shown in this paper, the above interpretation is not complete. An examination of the phase plane for the Fermi problem, which is presented in Sec. II, reveals a large number of adiabatic islands embedded in a nonadiabatic sea. Depending on the details of the wall motion, the fundamental island found by Zaslavskii and Chirikov is generally not the absolute barrier to stochastically heated particles, initially at lower energies. In fact, for smooth force functions, the absolute barrier exists at velocities far below that associated with the fundamental island.

In part, the technique for analytically examining the linear aspects of the Fermi problem is similar to one considered by Greene<sup>9</sup>: Determine the fixed points in the phase plane and examine the stability of the linearized motion about these singularities. If the fixed points represent elliptic singularities, and the Jacobian of the linearized motion is equal to unity, adiabatic orbits exist in the neighborhood of the fixed points. Otherwise the neighborhood of the singularities is generally accessible from the stochastic sea. From these considerations, we generally obtain a velocity boundary  $u_s$  in the phase plane below which no adiabatic regions exist. In

addition, we determine a simple lower bound on the stochastically accessible phase space. These questions are explored in some detail in Sec. III A and compared with the numerical results of Sec. II.

An alternative procedure for examining the adiabatic regions involves transforming the variables to a phase space in which the difference equations can be approximated by differential equations. First integrals give the Hamiltonian (adiabatic) trajectories, from which nonlinear motion in the neighborhood of the fixed points may be examined, yielding the nonlinear boundaries of the adiabatic regions. This is, in fact, the technique employed by Zaslavskii and Chirikov for the fundamental resonance between the bounce frequency and the wall-oscillation frequency. Higher harmonic and subharmonic resonances can equally well be examined by this procedure, revealing the entire island structure. The nonlinear stability of the adiabatic regions and the maximum velocity to which particles can be heated can also be determined approximately from higher-order resonance theory as developed by Jaeger and Lichtenberg.<sup>4</sup> These techniques are presented in Sec. III B.

Although the nonadiabatic or phase-filling trajectories have been called stochastic, this does not imply that the distribution function for the particle velocities can be determined by use of a random-phase assumption for particle-wall collisions. In the region of the phase plane in which adiabatic islands exist, the entire phase plane is not available to a nonadiabatic particle, and the random-phase assumption may be inapplicable. Even in the region of the phase plane where adiabatic islands do not exist, phase correlations may persist between successive wall collisions. An examination of these correlations and their effect on the calculation of the velocity space density distribution from the Fokker-Planck equation is the subject of Sec. IV.

The Fermi problem typifies a large class of acceleration problems which exhibit much of the same phase-space structure. There also can be some notable differences, particularly if the heating is described by a set of non-area-preserving equations. An example falling into this latter category is cyclotron-resonance heating in a magnetic mirror field. Where convenient, we contrast the results of an approximation to this acceleration mechanism with that of the Fermi problem.

## II. NUMERICAL RESULTS

We consider first the dynamics of a particle elastically bouncing between a fixed and a periodically oscillating wall, as shown in Fig. 1 (a). For the wall velocity given by a sawtooth function in time, Zaslavskii and Chirikov have obtained the following set of exact difference equations for the particle motion<sup>6</sup>:

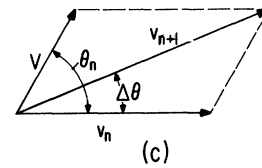
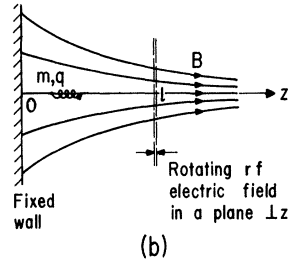
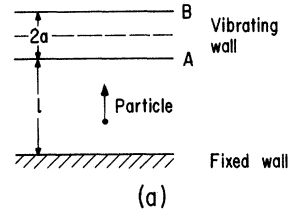


FIG. 1. (a) One-dimensional Fermi problem; (b) simplified cyclotron-heating problem; (c) relation between  $\vec{v}_n$  and  $\vec{v}_{n+1}$  for the cyclotron-heating problem.

$$u_{n+1} = \pm u_n + (\Psi_n - \frac{1}{2}), \quad (1)$$

$$\Psi_{n+1} = \frac{1}{2} - 2u_{n+1} + [(\frac{1}{2} - 2u_{n+1})^2 + 4\phi_n u_{n+1}]^{1/2} \quad (u_{n+1} > \frac{1}{4}\Psi_n), \quad (2)$$

$$\Psi_{n+1} = 1 - \Psi_n + 4u_{n+1} \quad (u_{n+1} \leq \frac{1}{4}\Psi_n), \quad (3)$$

$$\phi_n = \left\{ \Psi_n + \frac{\Psi_n(1 - \Psi_n) + l/4a}{4u_{n+1}} \right\}. \quad (4)$$

Here  $2a$  is the peak amplitude of the wall oscillation,  $l$  is the minimum distance between the walls,  $u_n$  is the velocity of the particle normalized to  $V$ , where  $\frac{1}{4}V$  is the amplitude of the velocity of the wall,  $n$  is the number of collisions with the moving wall,  $\Psi_n$  is the phase of the vibrating wall at the time of collision and changes from 0 to  $\frac{1}{2}$  as the wall moves from position A to position B and from  $\frac{1}{2}$  to 1 during the reverse motion, and brackets  $\{\dots\}$  denote the fractional part of the argument. The plus sign in Eq. (1) corresponds to Eq. (2) during the preceding step, and the minus sign to Eq. (3).

A simplification of Eqs. (1)–(4) can be realized if we allow the oscillating wall to impart momentum to the particle, according to its velocity, without physically changing its position in space. The problem defined in this manner has most of the features of the more physical problem and is also capable of generalization to other wall-forcing functions. We shall compare results of the two problems in the numerical calculations. For the simplified problem, the difference equations, in normalized form, become

$$u_{n+1} = \left| u_n + \Psi_n - \frac{1}{2} \right|, \quad (5)$$

$$\Psi_{n+1} = \left\{ \Psi_n + M/u_{n+1} \right\}, \quad (6)$$

where  $M = l/16a$ ,  $M/u = 2l/vT$  is the normalized transit time,  $T = 32a/V$  is the wall-oscillation period, and  $v = uV$ , the particle velocity.

We have introduced the absolute-value signs in Eq. (5) to correspond to the velocity reversal, at low velocities  $u < 1$ , which appears in the exact equations (1) and (3). This assumption has no effect on the region  $u > 1$ , which is the region of interest. These simplified equations can be obtained as an approximation to the exact set for  $l/a \gg 1$  and  $u \gg 1$ .

Equations (5) and (6) are readily generalized to nonlinear force functions; for example, for a cubic momentum transfer we have

$$u_{n+1} = \left| u_n + (2\Psi_n - 1) [1 - (2\Psi_n - 1)^2] \right|, \quad (7)$$

$$\Psi_{n+1} = \left\{ \Psi_n + M/u_{n+1} \right\}. \quad (8)$$

For a sinusoidal momentum transfer we find

$$u_{n+1} = \left| u_n + \sin \Psi_n \right|, \quad (9)$$

$$\Psi_{n+1} = \Psi_n + 2\pi M/u_{n+1}, \quad (10)$$

with the phase of the wall oscillation extending over  $2\pi$  rather than unity. As we shall see, the nonlinear force function is in many ways simpler than the linear one.

The difference equations (1)–(4), (5) and (6), (7) and (8), or (9) and (10) are readily solvable, for hundreds of thousands of wall collisions, on a high-speed computer. To explore the entire phase space, we divide the phase interval  $(0, 1)$  or  $(0, 2\pi)$  into 100 increments and the velocity interval  $(0, u_{\max})$  into 200 increments. We keep track of the number of times a particle is found within any of the 20 000 cells of the phase space. The results of the calculations for Eqs. (5) and (6), with  $M = 10$ , for ten particles, are given in Fig. 2, after 163 840 wall collisions per particle. Normalized velocity  $u$  is measured downward. The symbol in each cell represents the number of cell occupations according to Table I. A blank means zero occupations. The density distribution  $\bar{f}(u)$ , integrated over phases and over all collisions, is given to the left of the phase space. The particles are initially given phases and low velocities, chosen randomly. Subsequent collisions allow them to stochastically explore the phase space available. The final phase-plane plot is independent of the initial conditions of the particles. The unoccupied islands are bounded by adiabatic curves, and therefore are inaccessible from outside. The centers of the islands are elliptic singularities in the phase plane. Near these centers, the particle motion also traces out closed trajectories, as we shall discuss in Sec. III. We also show that for  $u < \frac{1}{2}M^{1/2}$ , the linearized motion

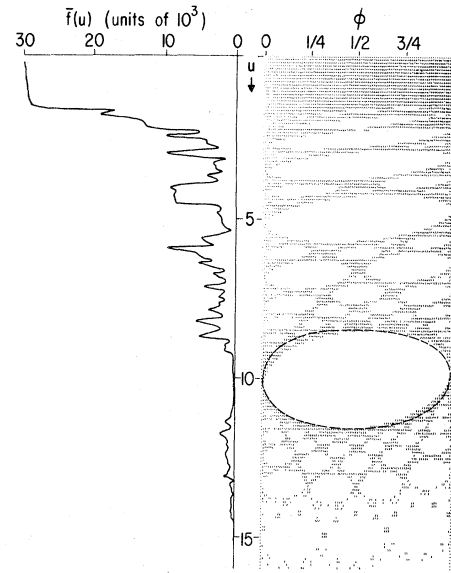


FIG. 2. Phase space  $u$ - $\phi$  and velocity distribution  $\bar{f}(u)$  for Eqs. (5) and (6), sawtooth wall velocity.  $M = 10$ , ten particles with 163 840 collisions/particle.

about all the principal singularities is unstable, as is readily verified from the numerical phase plot. The elliptic singular point of the main island at  $u/M = 1$  corresponds to one-to-one resonance between the particle oscillation and the wall oscillation. The successive central resonances at lower velocities  $u/M = \frac{1}{2}, \frac{1}{3}, \frac{1}{4}, \dots$ , correspond to the  $1-2, 1-3, 1-4, \dots$ , resonances, respectively. The other islands give the  $m-k$  resonances, where  $m$  and  $k$  are relatively prime integers. The positions of the elliptic singularities and the linearized motion around them are obtained in Sec. IIIA.

In Figs. 3 and 4, we repeat the calculation for the nonlinear wall velocity of Eqs. (7) and (8) and Eqs. (9) and (10), respectively. In Fig. 3,  $M = 10$ , with ten particles, for 81 920 collisions per particle. In Fig. 4,  $M = 100$ , with 622 592 collisions of a single particle. For these nonlinear velocities, the sizes of the adiabatic regions are diminished at low velocities owing to the presence of higher-order resonances between the period of the island trajectory and the average bounce period, as discussed in Sec. IIIB. An upper velocity boundary  $u_b$  (absolute barrier) also exists, beyond which the motion is adiabatic, so that no particles can penetrate from smaller velocities. The seeming contradiction of greater adiabaticity for nonlinear wall velocities is resolved if the discontinuities at the edge of the sawtooth wall velocity are included. Provided the motion is localized within one period of the phase (libration within the separatrix of an elliptic singularity), the sawtooth wave gives rise

TABLE I. Number of occupations in a phase-space cell as a function of the symbol in each cell.

Symbol	Number of cell occupations
blank	0
1	1-10
2	11-20
3	21-40
4	41-80
5	81-160
6	161-320
7	321-640
8	641-1280
9	1281-2560
*	above 2560

to stable motion for  $u > \frac{1}{2}M^{1/2}$ . However, outside of the separatrix, the drifting orbits encounter the wall-velocity discontinuities which destroy the adiabatic motion. The dashed curves in Figs. 2 and 4 show the separatrices for two island oscillations as calculated from Hamiltonian theory. With the linear force (Fig. 2) the separatrix is approximately an ellipse. With the sinusoidal force (Fig. 4) the trajectories near the separatrix are unstable, because of second-order island formation, as described in Sec. III B. For this case a Hamiltonian trajectory is also given that corresponds to a maximum phase excursion near the stability limit. The slight skewing of the islands in the numerically calculated plots arises from a term neglected in the Hamiltonian approximation of Sec. III B.

The qualitative features of the phase space are retained for arbitrarily large values of  $M$ . In Fig. 5 we give results of Eqs. (5) and (6) for  $M=1000$ . There are ten particles with 40 960 collisions per particle. The central islands occur at the same values of  $u/M$  as in the  $M=10$  example. We now see rather large values of  $u$  below which islands do not exist.

In Figs. 6 and 7, the phase space for the motion specified by Eqs. (1)-(4) is given, with  $M=1000$

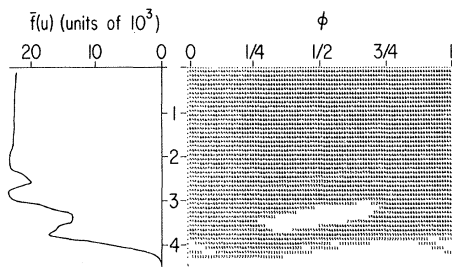


FIG. 3. Phase space  $u-\phi$  for Eqs. (7) and (8), cubic wall velocity.  $M=10$ , ten particles with 81 920 collisions/particle.

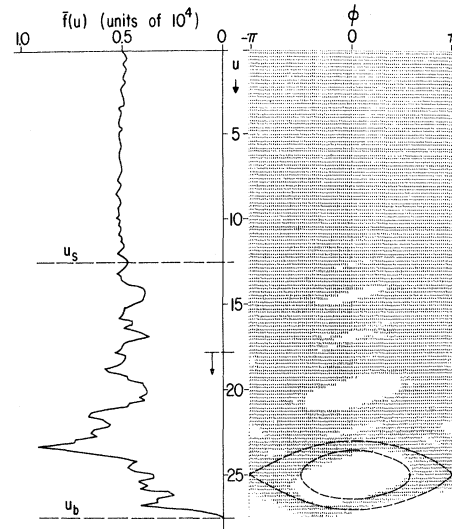


FIG. 4. Phase space  $u-\phi$  and velocity distribution  $\bar{f}(u)$  for Eqs. (9) and (10), sinusoidal wall velocity.  $M=100$ , 622 592 collisions of a single particle.

and  $M=10\,000$ , respectively, for ten particles, with 40 960 collisions per particle. Except at small  $u$ , the results are similar to those of the simplified problem equations (5) and (6). The difference in  $\bar{f}(u)$  within the stochastic region will be explored in detail in Sec. IV. Briefly, we can observe that a random-phase assumption as applied to Eqs. (1) or (5) would lead to a uniform velocity distribution. It is the departures from this assumption, embodied in higher-order phase correlations, that lead to the differing results for  $\bar{f}(u)$  in Figs. 5 and 6.

Numerically integrating Eqs. (1)-(4), Zaslavskii and Chirikov<sup>8</sup> obtained  $\bar{f}(u)$ , and recognized that an island existed at  $u=M$ . They postulated that a random-phase assumption was appropriate for  $u < M^{1/2}$ . In the intermediate velocity region  $M^{1/2} < u < M$ , they postulated further that the density fell off due to partial phase correlation. In fact, the density in velocity space falls off due to the existence of adiabatic islands in the phase plane. As we shall see in Sec. IV, the phase correlation results in modifications in the Fokker-Planck coefficients that may lead to an enhancement, rather than a diminution, of the density at higher velocities.

The procedures considered here are applicable to a wide class of problems associated with particles being acted upon by periodic forces, or more generally the behavior of differential and difference equations with periodic coefficients. One problem of practical interest is that of a charged particle confined in a magnetic mirror, interacting with a rf wave that is resonant with the particle gyrofrequency at some magnetic field within the contain-

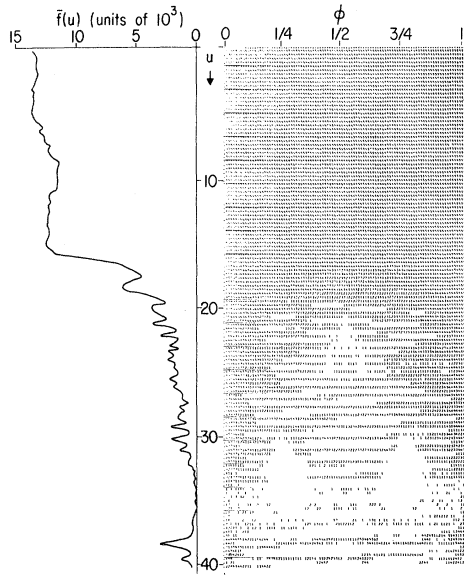


FIG. 5. Phase space  $u$ - $\phi$  and velocity distribution  $\bar{f}(u)$  for Eqs. (5) and (6), sawtooth wall velocity.  $M = 1000$ , ten particles with 40 960 collisions/particle.

ment region. As a simple model, we consider the longitudinal and transverse motion of a charged particle trapped in a linear magnetic field  $B_z(z) = B_0(1 + \alpha z)$ , as shown in Fig. 1(b). A perfectly reflecting wall at  $z=0$  reflects a negative-velocity particle back toward the positive  $z$  axis. The rf heating zone at  $z=l$  consists of a circularly polarized electric field lying in the  $x$ - $y$  plane, of negligible longitudinal extent, rotating at the local cyclotron frequency. The guiding-center approximation is used to describe the particle motion. As the particle is reflected back and forth in the mirror between  $z=0$  and  $z>l$ , it passes through the heating zone at  $z=l$ . The motion of the particle, assuming an impulsive transverse force in the heating zone, and assuming that the longitudinal velocity of the particle is zero at  $z=l+$ , is described by the following system of difference equations:

$$v_{n+1} = (v_n^2 + V^2 + 2v_n V \cos \theta_n)^{1/2}, \quad (11)$$

$$\theta_{n+1} = \theta_n + 2\pi M V / v_{n+1} + \Delta \theta, \quad (12)$$

where

$$\Delta \theta = \sin^{-1} \left( \frac{V \sin \theta_n}{v_{n+1}} \right), \quad v_n > -V \cos \theta_n$$

$$= \pi - \sin^{-1} \left( \frac{V \sin \theta_n}{v_{n+1}} \right), \quad v_n < -V \cos \theta_n. \quad (13)$$

$v_n$  is the magnitude of the transverse velocity of the particles,  $n$  is the number of collisions with the heating zone,  $\theta_n$  is the angle between the rf electric field and the transverse velocity vector of the particle just before a collision,  $V$  is the magnitude of

the velocity increment which the rf field imparts to the transverse velocity of the particle, and  $M = \frac{4}{3} [\alpha l + (\alpha l)^2]^{1/2} \omega_{c0} l / V$ , where  $\omega_{c0}$  is the cyclotron frequency at  $z=0$ . Figure 1(c) shows the geometrical relation between the various quantities in Eqs. (11)–(13) for this system.

In Fig. 8, the phase space is given for the cyclotron-resonance problem, with  $M = 57.8$ , with ten particles, after (a) 2560 and (b) 5120 collisions per particle. The phase space exhibits some features strikingly different from those observed in the Fermi-acceleration model. The low occupation numbers at low velocities indicate the presence of a strong frictional force which accelerates particles to higher energies. It is clear from the form of the phase plane and the way it changes with the number of collisions that there exist points in the phase plane which are sinks for particles. These sinks have replaced the adiabatic portions of the phase plane that excluded particles in the previous problems. There is also no maximum velocity  $u_b$  beyond which particles cannot be accelerated. At large  $u$ , the trajectories of the particles slant across the phase plane such that the particles march inexorably toward higher velocities. In Fig. 8, these effects can be clearly seen. Of the ten particles started at low velocities, one has been trapped in a double sink at  $u = 12$ , four in a sink at



FIG. 6. Phase space  $u$ - $\phi$  for the Zaslavskii-Chirikov equations (1)–(4), sawtooth wall velocity.  $M = 1000$ , ten particles with 40 960 collisions/particle.

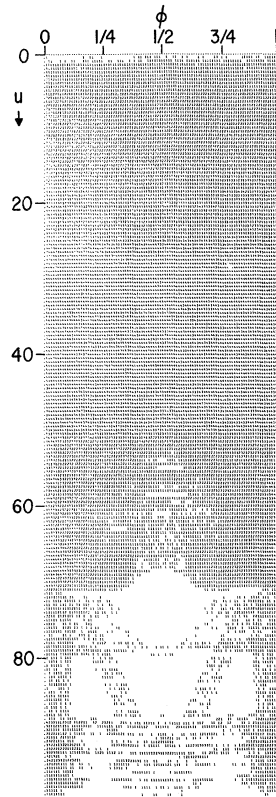


FIG. 7. Phase space  $u$ - $\phi$  for the Zaslavskii-Chirikov equations (1)-(4), sawtooth wall velocity.  $M=10\,000$ , ten particles with 40 960 collisions/particle.

28.9, and one in the sink (main island) at  $u=M=57.8$ . The other four particles have penetrated above  $u=M$ ; their velocities are observed to continuously increase in a nonstochastic fashion. The difference between the model of cyclotron-resonance acceleration and the Fermi-acceleration models, which accounts for the strikingly different trajectory behavior, rests on the fact that the phase-space mapping of the former is not area preserving. The mathematical exposition is given in Sec. III.

The force function may include a stochastic component in addition to the periodic component. We introduce such a component, modifying Eq. (6), for example, to

$$\Psi_{n+1} = \{\Psi_n + M/u_{n+1} + \Delta\Psi\}, \quad (14)$$

where  $\Delta\Psi$  is a random-phase shift. If  $\Delta\Psi$  is allowed to take on all phases between 0 and  $2\pi$ , we would expect the motion governed by Eqs. (5) and (6) to reduce to the usual random-walk problem, independent of the phase shift  $M/u_{n+1}$ , and this is indeed what is observed computationally. For a more restricted allowable region for  $\Delta\Psi$ , which corresponds to a weak stochastic force, the adiabatic regions are filled in, but on a slower time scale than that required for generating the island structure itself. In Fig. 9, we illustrate this behavior for  $-0.005$

$< \Delta\Psi < 0.005$ . We have chosen  $M=10$ , with ten particles, for (a) 10 240 and (b) 20 480 collisions per particle. For a small random component of the total force, the time scale for diffusion into the islands is longer than the time scale for the delineation of the adiabatic regions. As we see from Fig. 9, the smaller islands have been considerably filled in, while the larger islands have only been slightly modified. It is interesting to note that more densely occupied bands appear within the adiabatic region, corresponding to particles that have penetrated the adiabatic region due to the random-phase fluctuations, but have subsequently primarily followed the adiabatic orbits. These denser bands also appear in the stochastic portion of the phase space near an island where the particle trajectories are almost closed. On a sufficiently long time scale, governed by the statistics of the occupation numbers, one expects these bands to disappear.

### III. THEORY

#### A. Mappings for Difference Equations

Particle motion of the type we consider is described by a set of two first-order coupled difference equations:

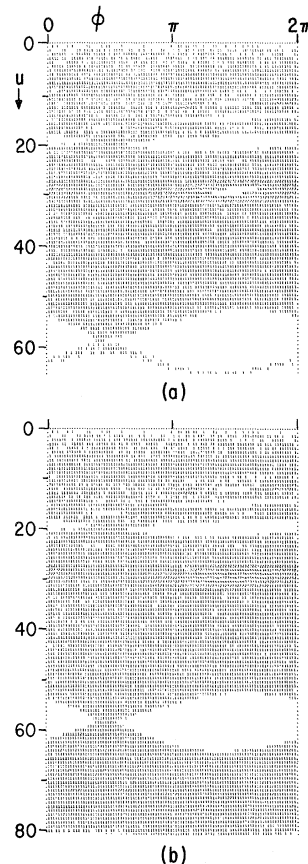


FIG. 8. Phase space  $u$ - $\phi$  for Eqs. (11)-(13), cyclotron heating.  $M=57.8$ , for ten particles, after (a) 2560 and (b) 5120 collisions/particle.

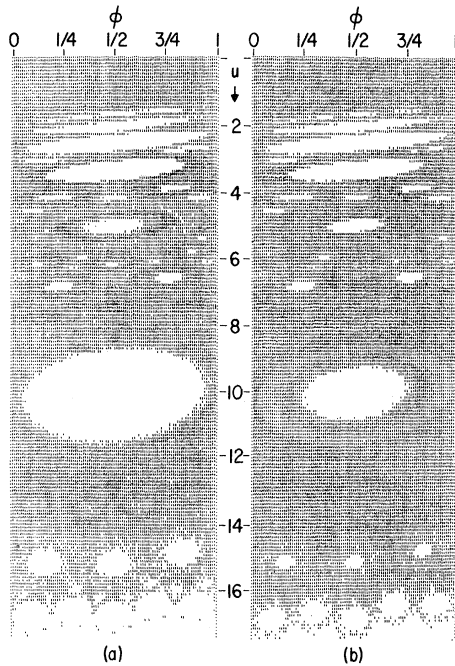


FIG. 9. Phase space  $u$ - $\phi$  for Eqs. (5) and (14), saw-tooth wall velocity with an additional weak stochastic force.  $M=10$ ,  $-0.005 < \Delta\Psi < 0.005$ . (a) 10240 and (b) 20480 collisions of a single particle.

$$u_{n+1} = u_n + F(u_n, \Psi_n), \quad (15)$$

$$\Psi_{n+1} = \Psi_n + A(u_{n+1}) + G(u_{n+1}, \Psi_n), \quad (16)$$

where  $F$  and  $G$  are periodic in  $\Psi_n$  with a period  $\Theta$  of  $2\pi$  (or sometimes, for convenience, unity), and  $F, G \rightarrow 0$  as the periodic force tends to zero. The function  $A$  is chosen to describe the advancing of the phase  $\Psi_n$  in the absence of the applied periodic force. It is useful to introduce the variable  $\phi_n = \Psi_n \text{ modulo } \Theta$ . The quantities  $u_n$  and  $\Psi_n$  are often conveniently chosen to be, respectively, the normalized velocity and phase (with respect to the force) of the particle just before its  $n$ th collision with the force. If the force acts continuously rather than impulsively on the particle, then a reference plane, for example,  $z = z_0$ , is chosen on which  $u_n$  and  $\Psi_n$  can be defined. It is often convenient to regard  $G$  as a function of  $u_{n+1}$  rather than  $u_n$ ; no loss of generality is involved.

Equations (15) and (16) define a mapping in a two-dimensional space  $\underline{p} = (u, \phi)$ , such that

$$\underline{p}_{n+1} = M(\underline{p}_n), \quad (17)$$

which can be iterated:

$$\underline{p}_{n+k} = M^k(\underline{p}_n). \quad (18)$$

The condition that the mapping (17) is area preserving is that  $\det(J) = 1$ . Here  $J(\underline{p}_n) = J(u_{n+1}, \phi_{n+1} | u_n, \phi_n)$  is the Jacobian matrix of the mapping, and

for Eqs. (15) and (16),

$$\det(J) = \left(1 + \frac{\partial F}{\partial u}\right) \left(1 + \frac{\partial G}{\partial \Psi}\right). \quad (19)$$

It is well known that a dynamical system describable by a Hamiltonian  $H(q_1 \cdots q_n, p_1 \cdots p_n, t)$  induces in the  $2n$ -dimensional phase space of the system an area- (measure-) preserving flow. Thus, if the mapping (17) is obtained directly from a one-dimensional Hamiltonian  $H(q_1, p_1, t)$ , it must be area preserving. The Zaslavskii-Chirikov equations (1)–(4) and their simple variants (5) and (6), (7) and (8), and (9) and (10) are examples of area-preserving mappings. For a three-dimensional Hamiltonian, it is sometimes possible, making use of one or more integrals of the motion, to obtain a reduced phase space of less than six dimensions which undergoes an area-preserving flow. However, this is often not the case. In general, the flow in a restricted phase space of two dimensions is not area preserving. The approximation to cyclotron-resonance heating given by Eqs. (11)–(13) is an example of a non-area-preserving mapping. It should be noted, however, that in other approximate treatments of the cyclotron-heating problem, for portions of the parameter space, sufficient invariants exist to recover the area-preserving property.<sup>10</sup>

*Fixed points.* Equations (15) and (16) possess a fixed point of order  $k$  at  $\underline{P} = (u, \phi)$  when  $\underline{P} = M^k(\underline{P})$  and  $\underline{P}$  is not a fixed point of any order less than  $k$ ; i. e., a particle located exactly at  $\underline{P}$  will reappear after  $k$  collisions. For every positive integer value of  $k$ , there is a denumerably infinite set of fixed points. Fixed points of order  $k$  occur in families of exactly  $k$  members each. These families of fixed points may be organized into a hierarchy, as discussed by Greene.<sup>9</sup>

To obtain all the  $k$ th-order fixed points, we solve the  $2k+2$  algebraic equations

$$\begin{aligned} u_{j+1} &= |u_j + F(u_j, \Psi_j)|, \\ \Psi_{j+1} &= \Psi_j + A(u_{j+1}) + G(u_{j+1}, \Psi_j), \quad j = 1, \dots, k \\ u_{k+1} &= u_1, \\ \Psi_{k+1} &= \Psi_1 \pm 2\pi m, \quad m = 0, 1, \dots \end{aligned} \quad (20)$$

where  $m$  is an integer relatively prime to  $k$ .

Let us consider the velocity and phase equations for the simplified Fermi problem:

$$u_{j+1} = |u_j + F(\Psi_j)|, \quad (21)$$

$$\Psi_{j+1} = \Psi_j + 2\pi M / u_{j+1}. \quad (22)$$

A few simple properties of these equations can be shown. Summing over the  $k+1$  velocity equations, and assuming  $u_j > F(\Psi_j)$  for all  $j$ , we obtain a relation among the phases for each family of fixed points:

$$\sum_{j=1}^k F(\Psi_j) = 0. \tag{23}$$

Summing over all  $k + 1$  phase equations, we obtain the "average" velocity  $\bar{u}_{km}$  of each family  $m$  of  $k$ th-order fixed points:

$$\bar{u}_{km} = kM/m,$$

where  $m$  is an integer relatively prime to  $k$ , and where

$$\bar{u}_{km}^{-1} = k^{-1} \sum_{j=1}^k u_j^{-1}.$$

For each  $k$ , the integer  $m$  is used to order the families of fixed points. The  $k$  members of each  $(k, m)$  family are all found within a velocity spread  $\Delta u_{\max} = (k - 1) |F|_{\max}$ .

As can be seen from Figs. 2-9, the most significant fixed points are those for  $u \gg 1$ , for which the quantity  $\epsilon = |F|_{\max} / \bar{u}_{km} \rightarrow 0$ . For  $\epsilon \equiv 0$ , the  $k$  members of each  $(k, m)$  family of fixed points are then located at  $(\Psi_j, u_j) = (\Psi_0 + 2\pi jm/k, kM/m)$ ,  $j = 1, \dots, k$ ,  $(m, k)$  relatively prime, where  $\Psi_0$  is arbitrary. The effect of a small but finite  $\epsilon$  is to determine the possible values for  $\Psi_0$ . For a finite  $\epsilon$ ,  $\Psi_0$  is obtained from Eq. (23):

$$\sum_{j=1}^k F\left(\Psi_0 + \frac{2\pi jm}{k}\right) = 0. \tag{24}$$

For a given  $k$ , this equation may have from none to an infinity of solutions, depending on the form of  $F$ . In the usual case,  $F$  has two zero crossings  $\theta_0, \theta_1$  ( $\theta_0 < \theta_1$ ) in the interval  $-\pi < \theta \leq \pi$ , and is anti-symmetric about  $\theta_0$ . It follows that  $\theta_1 = \theta_0 + \pi$  and that  $F$  is antisymmetric about  $\theta_1$ . In this case,  $\Psi_0 = \theta_0$  and  $\Psi_0 = \theta_0 + \pi/k$ ,  $k = 1, 2, 3, \dots$ . Some of these latter fixed points can easily be seen as the centers of the island structures in Figs. 2-9. In Table II, the calculated locations of the  $k = 1$  and some  $k = 2$  fixed points are given for the various acceleration problems considered here.

*Linearized mappings and stability.* It is of interest to study the stability of the particle motion in the immediate neighborhood of a fixed point  $\underline{P}_1$  of order  $k$ . Letting  $\Delta \underline{p}_n = \underline{p}_n - \underline{P}_1$ , we define a linearized mapping  $L$  by

$$\Delta \underline{p}_{n+k} = L \cdot \Delta \underline{p}_n. \tag{25}$$

Clearly,  $L$  is equal to the ordered product of  $k$  Jacobian matrices of  $M$ , each evaluated at the  $k$  successive fixed points of the family of which  $\underline{P}_1$  is a member,

$$L = J(\underline{P}_k) J(\underline{P}_{k-1}) \dots J(\underline{P}_1). \tag{26}$$

Under successive iterations of  $L$ , the particle moves in an orbit near the fixed point. To determine the character of the orbit, we solve the two linear difference equations (25) by introducing  $\Delta \underline{p}_{n+l k}$

TABLE II. Location and stability of  $k = 1$  and  $k = 2$  fixed points.

Problem	$k = 1$ fixed points		$k = 2$ fixed points	
	Location	Stability	Location	Stability
Zaslavskii-Chirikov equations (1)-(4), sawtooth wall velocity	$(\phi_1, u_1)$ , $m = 1, 2, 3, \dots$		$(\phi_1, u_1)$ and $(\phi_2, u_2)$ , $m = 1, 3, 5, 7, \dots$	
Approximate equations (5) and (6), sawtooth wall velocity	$(\frac{1}{2}, (M + \frac{1}{2}M^{-1}))$ $(\frac{1}{2}, M/m)$	stable if $u_1 > \frac{1}{2}(M + \frac{1}{2})^{1/2}$ stable if $u_1 > \frac{1}{2}M^{1/2}$	$(\frac{1}{3}, 2M/m + \frac{1}{3})$ and $(\frac{2}{3}, 2M/m - \frac{1}{3})$ , $u_1, u_2 \gg 1$	stable if $u_1 = u_2 > M^{1/2}$
Equations (9) and (10), sinusoidal wall velocity	$(0, M/m)$ $(\pi, M/m)$	stable if $u_1 > (\frac{1}{2}\pi M)^{1/2}$ hyperbolic (unstable)	some at $(\Psi_0, 2M/k)$ and $(\Psi_0 + \pi m, 2M/h)$ , where $\Psi_0 = \sin^{-1} 2M(m^{-1} - h^{-1})$ and $h = 1, 3, 5, \dots$	for $h = m$ , stable if $u_1 > (\pi M)^{1/2}$
Equations (11)-(13), simplified cyclotron heating	$(\frac{1}{2}(\pi + m/M), M/m)$ $(\frac{1}{2}(3\pi - m/M), M/m)$ , $u_1, u_2 \gg 1$	unstable trapped orbit if $u_1 > (\frac{1}{2}\pi M)^{1/2}$		
Equations (7) and (8), cubic wall velocity	$(\frac{1}{2}, M/m)$	stable if $u_1 > (\frac{1}{2}M)^{1/2}$		

$= \Delta p_0 r^i$ , and we obtain the following characteristic equation for  $r$ :

$$r^2 - r \operatorname{Tr}L + \det L = 0. \quad (27)$$

It is well known that the quantities  $\operatorname{Tr}L$  and  $\det L$  are invariant, independent of the cyclic order of the  $k$  Jacobian matrices in Eq. (26). Thus the roots of Eq. (27) are the same for all  $k$  fixed points in a given family.

The character of the solutions of Eq. (27) has been studied extensively in connection with nonlinear mechanics,<sup>11</sup> and we summarize the results below. For an area-preserving mapping  $M$ ,  $\det J = 1$ , and it follows from Eq. (26) that  $\det L = 1$ . For  $(\operatorname{Tr}L)^2 < 4$ , the two roots of Eq. (27) are complex conjugates and have unit magnitude:

$$r = e^{\pm i\theta}, \quad \cos \theta = \frac{1}{2} \operatorname{Tr}L. \quad (28)$$

In this case, the particle traces an elliptical orbit about the fixed point  $\underline{P}_1$ , completing one orbit every  $2\pi/\theta$  collisions. If, on the other hand,  $(\operatorname{Tr}L)^2 > 4$ , then the two roots of Eq. (27) are real, and one of them has a magnitude greater than unity. The particle traces one or both branches of a hyperbolic orbit, ultimately moving far from the fixed point. The character of these orbits (elliptic or hyperbolic) and the rotation angle  $\theta$  (if elliptic) is the same for all  $k$  members of the given family of fixed points. However, the actual shape and orientation of the orbit in the  $u$ - $\phi$  plane is different for each member of the family.

For mappings  $M$  which are not area preserving, the character of the orbits may be quite complex. For  $0 < \frac{1}{4}(\operatorname{Tr}L)^2 < \det L < 1$ , the two roots of Eq. (27) are complex conjugates, having a magnitude less than unity. The particle then spirals in toward the central fixed point ("trapped orbit"). Such orbits are responsible for the particle "sinks" seen in Fig. 8. For  $-1 + |\operatorname{Tr}L| < \det L < \frac{1}{4}(\operatorname{Tr}L)^2 < 1$ , a trapped orbit is also obtained, with the particle moving in toward the fixed point in a nonspiraling orbit. For  $\det L > \frac{1}{4}(\operatorname{Tr}L)^2 > 1$ , complex-conjugate roots having a magnitude greater than unity are obtained (unstable, spiraling-out motion). In all other cases, two real roots, one of which has a magnitude greater than unity, result. The orbit is then unstable.

*Stability of Fermi and cyclotron problems for  $k=1$  and  $k=2$ .* We now consider in detail the stability analysis for the problems shown in Table II. All of the Fermi problems are area-preserving mappings, while the cyclotron-resonance problem, Eqs. (11)–(13), is not. For the simplified sawtooth-wall-velocity problem, Eqs. (5) and (6), at the  $k=1$  fixed points (see Table II), we find  $\operatorname{Tr}L = 2 - m^2/M$ . An elliptic point (stable, closed orbit) is thus obtained if  $m < 2M^{1/2}$ , namely, if  $u_1 > \frac{1}{2}M^{1/2}$ . The rotation angle  $\theta$  is given by Eq. (28); for  $u_1$

$\gg M^{1/2}$ , we have  $\theta = m/M^{1/2} = M^{1/2}/u_1$ . For  $k=2$ ,  $u_1, u_2 \gg 1$ , we find  $\operatorname{Tr}L \approx 2 - m^2/M$ , and thus obtain stable orbits provided  $u_1 \approx u_2 > M^{1/2}$ . We note that as  $u$  is decreased from large toward small values, the  $k=2$  fixed points go unstable before the  $k=1$  fixed points. For the cubic wall velocity, Eqs. (7) and (8), one similarly obtains the stability condition for  $k=1$  that  $u_1 > (\frac{1}{2}M)^{1/2}$ . For the Zaslavskii-Chirikov mapping, Eqs. (1)–(4), for  $k=1$ , one obtains the condition for stable orbits  $u_1 > \frac{1}{2}(M + \frac{1}{8})^{1/2}$ . For the sinusoidal wall velocity, Eqs. (9) and (10), there are two  $k=1$  fixed points as shown in Table II, for each value of  $m$ . The fixed point at  $\phi_1 = \pi$  has  $\operatorname{Tr}L = 2 + 2\pi m^2/M$ , so that the orbits are unstable (hyperbolic) for all  $m$ . On the other hand, the fixed point of  $\phi_1 = 0$  has  $\operatorname{Tr}L = 2 - 2\pi m^2/M$ , so that these points are stable provided  $m < (2M/\pi)^{1/2}$ , i. e., provided  $u_1 > (\frac{1}{2}\pi M)^{1/2}$ . For  $k=2$ , a similar calculation shows that the fixed points  $\underline{P}_1 = (0, 2M/m)$  and  $\underline{P}_2 = (\pi, 2M/m)$  are stable, provided  $u_1 = u_2 > (\pi M)^{1/2}$ . We again note that, as  $u$  is decreased,  $k=2$  fixed points go unstable before the  $k=1$  fixed points.

The cyclotron-resonance heating problem, Eqs. (11)–(13), has two  $k=1$  fixed points for each value of  $m$ , as shown in Table II. For  $u_1 \gg 1$ , we obtain  $\operatorname{Tr}L$  and  $\det L$  as

$$\begin{aligned} \operatorname{Tr}L &= 2 \pm 2\pi m^2/M + O(u_1^{-4}), \\ \det L &= 1 - m^2/M^2 + O(u_1^{-4}), \end{aligned} \quad (29)$$

where the positive sign refers to the fixed point at  $\phi_1 = \frac{1}{2}(\pi + m/M)$  and the negative sign to the fixed point at  $\phi_1 = \frac{1}{2}(3\pi - m/M)$ . From the stability conditions, we find that the former fixed point is always unstable (hyperbolic), while the fixed point at  $\frac{1}{2}(3\pi - m/M)$  has trapped orbits (particle spirals into the fixed point) provided  $m < (2M/\pi)^{1/2}$ , namely, provided  $u_1 > (\frac{1}{2}\pi M)^{1/2}$ . For  $u_1 \gg M^{1/2}$ , the rotation angle  $\theta$  of the particle around the fixed point is approximately  $(2\pi M)^{1/2}/u_1$ . At the same time, the particle spirals exponentially in toward the fixed point as  $e^{-\beta n}$ , where the spiraling-in rate  $\beta = (2u_1^2)^{-1}$ . These trapped orbits can be seen very clearly in the phase-plane structure of Fig. 8. For convenience, the stability conditions for  $k=1$  and  $k=2$  are summarized in Table II.

*Stability for large  $k$ .* In general, the stability analysis for the  $k=3, 4, 5$ , etc., fixed points becomes progressively more difficult. However, by an expansion procedure, we can obtain an expression for the stability of fixed points for the simplified Fermi problem for large  $k$ . The Jacobian matrix of the mapping at  $(\phi_j, u_j)$ ,  $j=1, 2, \dots, k$ , is given by

$$J = \begin{bmatrix} 1 & F'_j \\ \delta_j & 1 + \delta_j F'_j \end{bmatrix}, \quad (30)$$

where  $\delta_j = -\Theta M/u_j^2$  and  $\Theta = 2\pi$  (or sometimes 1). Recalling that  $\bar{u}_{km} = kM/m$  and  $\Delta u_{\max} = (k-1)|F_{\max}$ , it is clear that we may write

$$\delta_j = \delta = -\Theta M/\bar{u}_{km}^2 = -\Theta m^2/k^2 M, \quad (31)$$

provided  $\Delta u_{\max} \ll \bar{u}_{km}$ , i. e., provided

$$|F|_{\max} \ll M/m. \quad (32)$$

For large  $k$ ,  $|\delta| \ll 1$ , and we can easily establish by induction, using Eq. (26), that

$$\text{Tr}L = 2 + k\delta \sum_{j=1}^k F'(\phi_j) + O(\delta^2). \quad (33)$$

Inserting Eq. (31) into Eq. (33) yields

$$\text{Tr}L = 2 - \frac{\Theta m^2}{kM} \sum_{j=1}^k F'(\phi_j). \quad (34)$$

If  $\sum F'$  is negative, then the fixed points are always unstable (hyperbolic). If  $\sum F'$  is positive, then stable orbits (elliptic fixed points) are obtained if

$$\sum F' < 4kM/\Theta m^2. \quad (35)$$

As an example, consider the sawtooth wall velocity, Eqs. (5) and (6), for which  $F'(\phi_i) = 1$  for all  $\phi_i$ , and the period  $\Theta = 1$ . Then  $\sum F' = k$ , and the  $k$ th-order fixed points have stable orbits provided  $m < 2M^{1/2}$ , or

$$\bar{u}_{km} > \frac{1}{2}kM^{1/2}. \quad (36)$$

At the stability boundary itself,  $\bar{u}_{km} = \frac{1}{2}kM^{1/2}$ ,  $\delta = -4/k^2$ , and  $M/m = \frac{1}{2}M^{1/2}$ . For  $k \geq 3$  and  $M \gg 1$ , both the assumption that  $|\delta| \ll 1$  and the inequality (32) are satisfied.

From Eq. (36) and the results listed in Table II, we see that the larger the value of  $k$ , the larger is the associated stability boundary  $u$ . It is clear that the  $k=1$  stability boundary represents an important transition velocity for a particle. Below this velocity, no adiabatic islands exist, and all phase-space states are accessible to low-velocity particles.

*Stochastic transition velocity  $u_s$ .* In addition to the above stability analysis for the sawtooth wall velocity, numerical computations of the nonlinear difference equations (15) and (16), for a wide variety of forcing functions  $F$ ,  $G$ , and with  $A(u_{n+1}) = 2\pi M/u_{n+1}$ , show the existence of a transition velocity  $u_s$  below which no adiabatic islands or (for non-area-preserving mappings) trapped orbits are observed. Figures 2-9 all show evidence of this transition velocity. We hypothesize that, except for pathological cases, a transition of this type always exists. Below  $u_s$ , all phase-space states are accessible to low-velocity particles. Above  $u_s$ , disjoint areas in phase space exist, with either no (area-preserving) or only one-way (non-area-preserving) access among these areas. Since a minimal requirement

for a stochastic description of particle motion in a given region of phase space is that all positions in phase space be accessible and have access to all other positions, we refer to  $u_s$  as a stochastic transition velocity; below  $u_s$ , a stochastic description of the motion may be possible, as described in Sec. IV.

To calculate the value of  $u_s$ , one must in principle examine the character of the orbits around families of fixed points of all orders  $k$ . However, numerical computations and analytical results for the sawtooth wall velocity suggest that the stochastic barrier  $u_s$  is associated with the stability or instability of the  $k=1$  fixed points of the mapping  $M$ . It is thus sufficient to calculate the stability boundary of the  $k=1$  fixed points. A comparison of the calculated stability boundaries for  $k=1$  with the computational result for  $u_s$  is shown in Fig. 10, for various wall-velocity functions and values of  $M$ .

A physical interpretation of the transition velocity  $u_s$  can be obtained by observing that the stability boundary occurs at  $\cos\theta = -1$  in Eq. (28); i. e., the phase shift per bounce of the island oscillation around the fixed points is equal to  $\pi$ . This is just the well-known condition for stop bands in a periodic structure. In terms of the period  $\tau_i$  of the island oscillation,  $\tau_i < 2\tau_b$  for stochasticity, where  $\tau_b$  is the bounce period. Setting  $\theta = \pi$  in Eq. (28), we can determine the ordering of the natural periods for stochasticity,  $\tau_b > (V\pi F')^{-1} \nu \tau_{\text{wall}}$ , where, typically,  $\pi F'$  is of order unity.

*Absolute barrier velocity  $u_b$ .* An examination of Figs. 2-9 shows that, for certain mappings, an impenetrable velocity barrier  $u_b$  exists, above which particles initially at low velocities can never be subsequently heated. This barrier does not exist for the cyclotron-heating problem, because the mapping is not area preserving. Particles which penetrate to  $u > M$  are thereafter continuously heated. For the sawtooth wall velocity, either Eqs. (1)-(4)

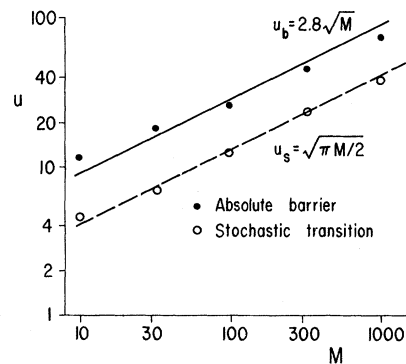


FIG. 10. Absolute barrier  $u_b$  and stochastic transition velocity  $u_s$  as a function of  $M$ , for the sinusoidal wall velocity of Eqs. (9) and (10).

or Eqs. (5) and (6), the barrier also does not exist, due to the discontinuous nature of the wall velocity. However, in this case, for a finite number of collisions,  $\bar{f}(u)$  drops off sharply for some  $u > \frac{1}{2}M^{1/2}$ , since the particle can only penetrate considerably beyond this value of  $u$  near the discontinuity at  $\phi = 0$  or  $1$ . For an area-preserving mapping with a smooth wall velocity, such as Eqs. (7) and (8) or Eqs. (9) and (10), the absolute barrier always exists. This barrier curve, located at  $u_b$ , is the Arnol'd-Moser invariant curve<sup>12,13</sup> of the mapping equations (15) and (16), having the lowest average value of  $u$ . Arnol'd and Moser have shown that, given suitable smallness conditions on the derivatives of  $F$ ,  $G$ , and  $A$ , invariant curves of the mapping always exist. In practice, their existence proofs are of little use in predicting the location  $u_b$  of an absolute barrier.<sup>13</sup> However, for the Fermi problem, we can obtain a lower bound on the location of the absolute barrier  $u_b$  as described below. In Sec. III B, we approximately determine its location by Hamiltonian techniques.

To find the lower bound, we insert the transformation  $w = 2\pi M/u$  into Eqs. (21) and (22). We obtain

$$w_{n+1} = w_n + H(w_n, \Psi_n), \quad (37)$$

$$\Psi_{n+1} = \Psi_n + w_{n+1}, \quad (38)$$

$$H(w_n, \Psi_n) = -w_n^2 F(\Psi_n) / [2\pi M + w_n F(\Psi_n)]. \quad (39)$$

If we introduce the rotation angle  $\Omega(\phi)$  and the radius  $w(\phi)$ , which parametrize the assumed invariant curve in  $\phi$ , we find from Eqs. (37) and (38) that

$$\Omega(\phi) = w(\phi) + H(w(\phi), \phi), \quad (40)$$

$$\Omega(\phi) = w(\phi + \Omega(\phi)). \quad (41)$$

We impose the condition that  $\Omega$  and  $w$  be continuous single-valued functions of  $\phi$ ; i.e., breakup of the invariant curve into islands or a double-valued invariant curve does not exist. Differentiating Eqs. (40) and (41), we find

$$\Omega_\phi = w_\phi + H_w w_\phi + H_\phi, \quad (42)$$

$$\Omega_\phi = w_T (1 + \Omega_\phi), \quad (43)$$

where the subscripts  $w$  and  $\phi$  denote differentiation with respect to that variable, and  $w_T$  is  $w_\phi$  evaluated at  $\phi + \Omega(\phi)$ .

It is clear from Eq. (43) that  $\Omega_\phi > -1$  and  $w_\phi < 1$ ; otherwise  $w$  and  $\Omega$  are not continuous single-valued functions of  $\phi$ . We can then form a necessary condition for the existence of an invariant curve:

$$-(1 + H_\phi)/(1 + H_w) < w_\phi < 1, \quad (44)$$

where the left-hand inequality in Eq. (44) is obtained by substituting the smallest possible value of  $\Omega_\phi$ ,  $-1$ , in Eq. (42). [Note that by Eq. (39),  $H_w > -1$ .] From Eq. (44), a sufficient condition that an invariant curve does not exist is

$$H_w + H_\phi < -2 \quad (45)$$

for some  $\phi$  in the range  $-\pi < \phi \leq \pi$ . As an example, consider  $F(\phi) = \sin\phi$ . Then

$$H_w + H_\phi = \frac{u^{-2} \cos^2 \phi - 2u^{-1} \sin \phi - 2\pi M u^{-2} \cos \phi}{(1 + u^{-1} \sin \phi)^2}.$$

Putting  $\phi \approx 0$  to make  $H_w + H_\phi$  as negative as possible, Eq. (45) yields  $u = (\pi M)^{1/2}$ . For velocities below this value, an invariant curve (absolute barrier  $u_b$ ) does not exist. Particles can be heated to at least a velocity  $(\pi M)^{1/2}$  under the influence of the periodic wall velocity. As can be seen from Figs. 4 and 10, the lower bound  $(\pi M)^{1/2}$  is within a factor of 1.5 of the actual barrier velocity  $u_b$ .

#### B. Hamiltonian Form of Fermi Problem with Sinusoidal Wall Velocity

The difference equations can be represented as differential equations by introduction of the singularity function in the force equation:

$$\frac{du}{d\tau} = \sum_{m=-\infty}^{\infty} e^{i2\pi m\tau} \sin \Psi \quad (46)$$

and

$$\frac{d\Psi}{d\tau} = \frac{2\pi M}{u}, \quad (47)$$

where the time variable  $\tau$  is measured in units of the number of wall collisions  $n$ , and the Fourier representation of the  $\delta$  function has been employed. Equations (46) and (47) have the Hamiltonian form

$$H(\tau) = 2\pi M \ln u + \sum e^{i2\pi m\tau} \cos \Psi, \quad (48)$$

with  $u$  and  $\Psi$  the canonical coordinates.

*Averaged equations.* For very large  $u$  ( $u \gg M$ ),

$$(u_{n+1} - u_n)/u_n \ll 1 \quad (49)$$

and

$$(\Psi_{n+1} - \Psi_n)/2\pi \ll 1, \quad (50)$$

allowing Eq. (48) to be averaged over  $\tau$  to obtain a first integral of the motion  $2\pi M \ln u + \cos \Psi = C$ . However, velocities this large are not of major interest to us, as can be seen from Figs. 2-9. For the velocity range of interest,  $1 \ll u \leq M$ , Eq. (50) is not satisfied, while Eq. (49) is. However, if we introduce a change in variable

$$\hat{u} = u - M/m, \quad \hat{\phi} = \Psi - 2\pi m\tau, \quad m \text{ an integer} \quad (51)$$

so as to transform to a coordinate system around a  $k=1$  fixed point at  $u_0 = M/m$ , then  $(\hat{\phi}_{n+1} - \hat{\phi}_n)/2\pi \ll 1$ . In the caret variables, Eqs. (46) and (47) take the form

$$\frac{d\hat{u}}{d\tau} = \sum e^{i2\pi m\tau} \sin \hat{\phi}, \quad (52)$$

$$\frac{d\hat{\phi}}{d\tau} = -\frac{2\pi M}{u_0^2} \hat{u}. \quad (53)$$

Equations (52) and (53) can be integrated to obtain the Hamiltonian

$$H = \frac{2\pi M}{u_0^2} \frac{\hat{u}^2}{2} - \sum e^{i2\pi m\tau} \cos\hat{\phi} = C . \quad (54)$$

If the motion in the  $\hat{u} - \hat{\phi}$  phase plane is assumed to be slow on the time scale  $\tau$ , Eq. (54) can be averaged over  $\tau$  to give the averaged Hamiltonian

$$\bar{H} = \frac{2\pi M}{u_0^2} \frac{\hat{u}^2}{2} - \cos\hat{\phi} = C , \quad (55)$$

which describes the trajectories near the main ( $k=1$ ) fixed points at  $\hat{\phi} = 0, \pi$ , and  $u = u_0$ . Near the elliptic singular point at  $\hat{\phi} = 0$ , the Hamiltonian curves of  $\bar{H}$  consist of encircling orbits out to the separatrix (hyperbolic singular point), beyond which there are drifting orbits. The maximum oscillation of  $u$  occurs for the separatrix trajectory, for which  $C$  has its maximum value of  $C = +1$ . From Eq. (55),

$$(\Delta u)_{\max} = 2u_0(2\pi M)^{-1/2} . \quad (56)$$

The Hamiltonian curves from Eq. (55) can be compared with the results from the numerical calculations. These results are shown as the dashed lines in Fig. 4. Near the fixed point, the linearized solution of the difference equations (25) are in agreement with the numerical calculations and the Hamiltonian curves.

*Estimate of absolute barrier.* The validity of the phase-space trajectories obtained from the averaged Hamiltonian is limited by second-order resonances between the wall-collision frequency and harmonics of the frequency of oscillation about the fixed points. For the linearized motion, the minimum value of  $u$  for stable oscillations was calculated in Sec. III A. The nonlinear stability (breakup into islands) is now investigated by use of Eqs. (54) and (55), in the manner described in detail in Ref. 4. We note from Eq. (55) that the linear frequency of oscillation about the elliptic singular point is  $\omega_0 = (2\pi M)^{1/2}/u_0$ , which is to be compared with the bounce frequency of  $2\pi M/u_0$ . For  $2\pi M \gg 1$  and  $2\pi M/u_0 = O(1)$ , resonances involve only high harmonics of the motion in the  $\hat{u} - \hat{\phi}$  phase plane. Except possibly near the separatrix, these harmonics have very small amplitudes, which lead to significant perturbations of the Hamiltonian curves as obtained from Eq. (55), only in the immediate vicinity of the resonances. Thus, we expect no significant nonlinear breakup of the invariant curves in this region. On the other hand, for  $2\pi M/u_0 = O(M^{1/2})$ , the phase plane, as obtained from Eq. (54), exhibits chains of islands with significant amplitudes, formed by alternating elliptic and hyperbolic fixed points. These islands break the smooth trajectories calculated from Eq. (55) at those values of  $C$  for which resonances occur. The lowest harmonic number resonance occurs

at a frequency near  $\omega_0$ , with successively higher harmonics resonating at values of  $C$  for which the "soft-spring" nonlinearity  $\cos\hat{\phi}$  in Eq. (55) sufficiently reduces the frequency.

Two types of orbits need to be examined: libration for which  $\hat{\phi}$  oscillates and rotation for which  $\hat{\phi}$  advances or retards continuously. The former are the orbits inside the separatrices joining the hyperbolic singular points of Eq. (54), and the latter are the orbits outside the separatrices. If the successive chains of islands do not interact strongly, i. e., do not have nearly overlapping amplitudes, then between the resonances, phase trajectories as given by Eq. (55) isolate the resonant regions of the phase plane from each other. The isolation achieved by the rotation orbits is physically more important, since the lowest-velocity adiabatic orbit isolates the stochastic region of the phase plane which can be explored by a single initially low-velocity trajectory from the remainder of the phase plane; i. e., the lowest-velocity adiabatic orbit is the absolute barrier  $u_b$ . Generally, the amplitudes of successively higher-order resonant island chains rapidly decrease, such that only the amplitudes of the second-order resonances need be examined.

The second-order island chains are calculated by a procedure developed by Jaeger and Lichtenberg,<sup>4</sup> to determine the breakup of the libration orbits. We apply the technique here to the rotation orbits. The average precession frequency is determined by transformation of the averaged Hamiltonian of Eq. (55) to action-angle variables by solving the Hamilton-Jacobi equation

$$\frac{2\pi M}{2u_0^2} \left( \frac{\partial S}{\partial \hat{\phi}} \right)^2 - \cos\hat{\phi} = C , \quad (57)$$

where the action is, by definition,

$$J = \frac{1}{2\pi} \int_{-\pi}^{\pi} u d\hat{\phi} ,$$

and the new and old variables are related by the usual relation  $\hat{u} = \partial S / \partial \hat{\phi}$  and  $\theta = \partial H / \partial J$ . For  $C > 1$  (rotation orbits),  $S$  may be solved in terms of elliptic integrals, and to lowest order in the nonlinearity,

$$H(J, \theta) = \pi M J^2 / u_0^2 = C , \quad (58)$$

with angular rotation frequency  $\omega = 2\pi M J / u_0^2$ . The transformation leading to Eq. (58) is performed on Eq. (54), the Hamiltonian before averaging. If the lowest harmonic resonant term is the  $l$ th harmonic of  $\theta$  resonating with the  $m$ th harmonic of  $\tau$ , then the generating function

$$W = (l\theta - 2\pi m\tau) \hat{J} \quad (59)$$

transforms the Hamiltonian to new variables  $\hat{\theta} = l\theta - 2\pi m\tau$  and  $\hat{J} = J/l$ , such that in the  $\hat{\theta} - \hat{J}$  phase plane, the resonance appears as a singularity about

which  $\hat{\theta}$  is slow compared to all other frequencies. An average over  $\tau$  then yields

$$\hat{H} = \frac{\pi M}{u_0^2} l^2 \hat{J}^2 - 2\pi m \hat{J} - A_l \frac{\pi M}{u_0^2} l^2 \hat{J}^2 \cos \hat{\theta} = C, \quad (60)$$

where  $A_l$  is the coefficient of the  $l$ th harmonic obtained from the nonlinear expansion of the Hamiltonian in terms of elliptic integrals. Within a numerical factor of order unity,  $A_l$  is given by

$$A_l \approx \frac{l}{2^{2l}} \left( \frac{2}{C+1} \right)^{2l}. \quad (61)$$

Assuming  $A_l \ll 1$ , Eq. (60) has elliptic and hyperbolic singular points at  $\bar{J} = u_0^2 m / M l^2$  and  $\bar{\theta} = 0$  and  $\pi$ , respectively, and the maximum excursion of  $\hat{J}$  is  $\Delta \hat{J}_{\max} = (2A_l \bar{J}^2)^{1/2}$ . The strength of the singularity is measured by comparing the shift in frequency due to the resonance,  $\Delta \omega_{\max} = (\partial \omega / \partial J) \Delta \hat{J}_{\max}$ , with the separation of resonances  $\delta \omega \approx \omega_0 / l$ . From Eq. (58),  $\partial \omega / \partial J = \omega_0 / \bar{J}$ , giving

$$\frac{\Delta \omega_{\max}}{\delta \omega} = 2^{1/2} l^{3/2} (C+1)^{-l}. \quad (62)$$

We note that Eq. (62) is a function of  $l = 2\pi / \omega_0$ , and from Eq. (58),

$$\omega_0 = 2(\pi M C)^{1/2} u_0,$$

such that  $l$  is a function of the ratio  $u_0 / M^{1/2}$ . Therefore, the absolute barrier occurs at a value of  $u_0 = KM^{1/2}$ , where  $K$  is a function of  $C$ , but independent of  $M$ .

The value of  $K$  can be obtained, approximately, from Eq. (62) by constructing Table III. Jaeger and Lichtenberg have shown in a number of numerical examples that island breakup occurs for  $\Delta \omega_{\max} / \delta \omega$  between 0.3 and 0.5. This indicates a range of values of  $l$  and  $C$  from Table III for which breakup can occur, but that the boundary must occur for  $C < 2$ . Unfortunately it is in this region that higher-order nonlinearities become important and the period becomes longer, with infinite period ( $l = \infty$ ) at the separatrix at  $C = 1$ . However, over a reasonable range of the higher-order nonlinearity, we might expect that  $\Delta \omega_{\max} / \delta \omega$  would not differ much from the data in Table III. Assuming that island breakup ceases to occur for  $\Delta \omega_{\max} / \delta \omega < 0.3$ , and setting  $C = 1.5$ , we obtain a value of  $K = 2.75$ . For permissible values of  $C$  in this neighborhood,  $K$  varies only slowly. We compare this result with

TABLE III.  $\Delta \omega_{\max} / \delta \omega$  for various values of  $C$  and  $l$ .

$C \setminus l$	2	3	4	5	6
1	1	0.91	0.7	0.49	0.31
1.5	0.65	0.46	0.3	0.16	
2	0.25	0.27	0.14		

the numerical values at which an absolute barrier is observed in Fig. 10, which gives the predicted linear relation between  $u_0$  and  $M^{1/2}$ , with  $K \approx 2.8$ .

A calculation similar to the above, performed for the closed orbits of the main island resonances, indicates that serious erosion of the elliptic trajectories occurs at comparable values of  $u_0$ . Thus the nonlinear effects have substantially equivalent roles in determining the transition from adiabatic to stochastic behavior for the orbits of libration and rotation. This result is in marked contrast to the trajectories of Eqs. (5) and (6), for which  $F(\phi) = \phi \text{ Mod } 1$ . In the latter case, the elliptic orbits are nearly linear, giving adiabatic orbits around stable fixed points that extend to the neighborhood of the separatrix. The rotation orbits, on the other hand, are not adiabatic, since the discontinuity of  $F(\phi)$  at the edges  $\phi = 0$  and  $\phi = 1$  introduces large amplitude perturbations in all harmonics of the rotation frequency. This behavior can be observed by comparison of Figs. 2 and 4. In Fig. 2, for  $F(\phi) = \phi \text{ Mod } 1$ , the main stable regions are observed out to the boundaries of the phase interval (hyperbolic fixed points) but no absolute barrier (adiabatic rotation trajectory) is observed. In Fig. 4, for  $F(\phi) = \sin \phi$ , in contrast, the area of the main adiabatic region, at values of  $u$  lower than the absolute barrier, is significantly reduced from that predicted from the Hamiltonian equation (55).

#### IV. STOCHASTIC ACCELERATION

In this section, we investigate in what sense the evolution of the velocity distribution function can be described by a stochastic process. Clearly the motion in the two-dimensional phase plane is deterministic. However, provided  $u < u_s$ , so that adiabatic islands do not exist, it may be possible to express the evolution of  $f(u, n)$ , the distribution in  $u$  alone, in terms of a Markov process in  $u$ <sup>14</sup>:

$$f(u, n) = \int f(u - \Delta u, 0) P(u - \Delta u, n | u) d(\Delta u), \quad (63)$$

where  $P$  is the conditional probability of a particle being at  $u$  if it were at  $u - \Delta u$ ,  $n$  collisions earlier. All quantities in Eq. (63) are independent of phase. If we make the additional assumption that  $n \gg 1$  and that  $\Delta u \ll u$ , i. e., that there exists a collision number  $n$  such that

$$1 \ll n \ll u / |F|_{\max}, \quad (64)$$

then Eq. (63) can be written in the form of a Fokker-Planck equation,

$$\frac{\partial f}{\partial n} = - \frac{\partial}{\partial u} (Bf) + \frac{1}{2} \frac{\partial^2}{\partial u^2} (Df), \quad (65)$$

where the frictional coefficient is

$$B(u) = (1/n) \int \Delta u P(u - \Delta u, n | u) d(\Delta u) \quad (66)$$

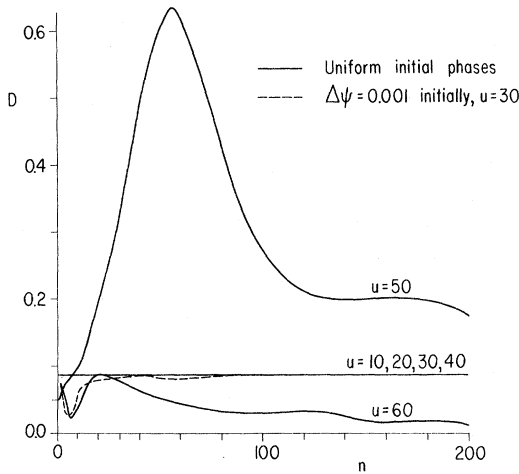


FIG. 11. Diffusion coefficient  $D$  as a function of  $n$  for Eqs. (5) and (6), sawtooth wall velocity.  $M = 10\,000$ , with 1000 particles placed at various initial velocities  $u_0$ , with random phases.

and the diffusion coefficient is

$$D(u) = (1/n) \int (\Delta u)^2 P(u - \Delta u, n | u) d(\Delta u). \quad (67)$$

*Validity of Fokker-Planck equation.* Of course,  $P$  is actually a function of the initial phase distribution as well as the initial velocity  $u - \Delta u$ . However, we expect that a correlation "time"  $n_c$  (measured in number of collisions) exists, such that any reasonably smooth initial phase distribution relaxes to a uniform phase distribution after approximately  $n_c$  collisions. Provided  $n$  can be chosen considerably larger than  $n_c$ ,  $P$  will be independent of the initial phase distribution. To estimate  $n_c$ , we use Eq. (30) to obtain

$$\Delta u_{n+1} = \Delta u_n + F' \Delta \phi_n, \quad (68)$$

$$\Delta \phi_{n+1} = -R \Delta u_n + (1 - RF') \Delta \phi_n,$$

where  $R = \Theta M / (u + F)^2$ . Below the stochastic transition velocity  $u_s$ ,  $R$  is greater than 2. In the worst case, we assume that the initial phases are spread over a small interval  $\Delta \phi(0)$ , and that  $\Delta u(0) = 0$ . Provided  $R \gg 1$ , the dominant terms in Eq. (68) then yield  $\Delta \phi(n) \approx R^n \Delta \phi(0)$  and  $\Delta u(n) \approx F' \times R^{n-1} \Delta \phi(0)$ . Setting the phase spread  $\Delta \phi(n)$  equal to the phase interval  $\Theta$  (1 or  $2\pi$ ), we find

$$n_c = \frac{\ln[\Theta / \Delta \phi(0)]}{\ln R}, \quad (69)$$

showing the weak logarithmic dependence of  $n_c$  on the initial phase interval, and thus on the form of the initial phase distribution. In contrast, since  $\Delta u(n_c) \ll u$ , the velocity distribution remains constant while phase randomization occurs. Provided  $n \gg n_c$  and inequality (64) is satisfied, the Fokker-Planck description of the time evolution of  $f$  is valid, and the Fokker-Planck coefficients  $B$  and

$D$  can be obtained from a random-phase assumption.

For  $u > u_s$ , invariants exist which relate velocity and phase, independent of time. Such invariants exist within the adiabatic islands, which cannot therefore be described by Eq. (63). In the sea surrounding the adiabatic islands, the process may be Markoffian in  $u$ , but the random-phase assumption is clearly not appropriate, as all phases are not available at a given velocity.

Making the simplest assumption that  $n = 1$ , for Fermi acceleration given either by Eqs. (1)–(4) or (5) and (6), and assuming all phases equally probable, we find  $B = 0$  and  $D = \frac{1}{12}$ . In Fig. 11, we compare the above analytical result using the random-phase assumption to the value of  $D$  obtained numerically as a function of  $n$  for 1000 particles placed at various initial values of velocity  $u$ . Equations (5) and (6) are used for the computation, with  $M = 10\,000$  and a stochastic transition boundary predicted at  $u_s = 50$ . For  $u = 10, 20, 30$ , and  $40$  and initially uniformly distributed phases, the phase correlation is found to be negligible, so that  $D(u, n) = D(u, 1) = \frac{1}{12}$  for  $n > 1$ . For  $u = 50$ , on the other hand, there is strong phase correlation, so that  $D$  is not independent of  $n$ , even for  $n \geq 200$ . For  $u = 60$ , another process also enters, as a number of the particles are initially trapped in adiabatic regions and do not take part in the diffusion process. Finally, if particles are not initially spread over all phases, there is a transient behavior for the first few  $n_c$  collisions, during which phase randomization is occurring, as seen from the dashed curve in Fig. 11.

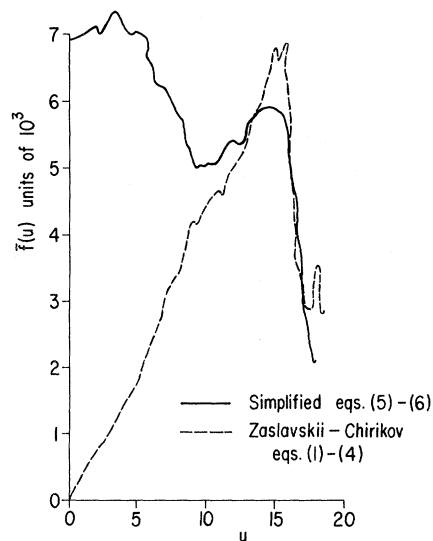


FIG. 12. Comparison of velocity distribution  $\bar{f}(u)$  for the Zaslavskii-Chirikov equations (1)–(4) and the simplified equations (5) and (6), for  $M = 1000$ .

*Steady-state solution and frictional coefficient*  
*B.* For the Fermi-acceleration mechanism, the small phase correlations which appear for  $n > 1$  do not significantly alter the diffusion coefficient. However, since  $B \equiv 0$  for  $n = 1$ , they may be of great importance in determining the frictional coefficient and ultimately the distribution function integrated over collisions,  $\bar{f}(u)$ .

Figure 12 shows a comparison of the velocity distribution  $\bar{f}(u)$  between the Zaslavskii-Chirikov problem [Eqs. (1)–(4)] and the simplified problem [Eqs. (5) and (6)]. The frictional coefficient can be determined from the numerical calculations of  $\bar{f}$  as follows: We assume perfectly reflecting barriers at  $u = 0$  and  $u = u_s$ , such that  $-Bf = \frac{1}{2} \partial(Df)/\partial u$  at  $u = 0, u_s$ . The steady-state ( $\partial/\partial n \equiv 0$ ) solution of Eq. (65) with these boundary conditions and with  $\bar{f}$  specified at  $u = u_0$  is

$$f(u, n \rightarrow \infty) = \bar{f}(u) = \bar{f}(u_0) D(u_0) D^{-1}(u) \times \exp \int_{u_0}^u 2B(u') D^{-1}(u') du', \quad (70)$$

from which we obtain, for  $D(u) = \frac{1}{12}$ ,

$$B(u) = \frac{1}{24} \frac{d(\ln \bar{f})}{du}. \quad (71)$$

For the Zaslavskii-Chirikov equations, from Fig. 12,  $\bar{f}(u) \propto u$ , so that from Eq. (71) we obtain  $B = (24u)^{-1}$ . This value of  $B$  is in rough agreement with an analytical calculation for  $n = 2$ , as follows:

Assuming  $u \gg 1$ , from Eqs. (1), (2), and (4), we obtain

$$u_{n+2} = u_n + \Psi_n - \frac{1}{2} + (1 + \frac{1}{4} u^{-1}) \{ \Psi_n + M/u_{n+1} \} - \frac{1}{2}. \quad (72)$$

For  $u^2 < M$   $\{\}$  is a rapidly varying function of  $u$  and  $\Psi$ . Averaging over  $\Psi$  and a small velocity interval  $\Delta u \approx 1$  yields  $\langle \{\} \rangle \approx \frac{1}{2}$ . From Eq. (72) we obtain  $B(u) = (16u)^{-1}$ . For the simplified equations (5) and (6), in the same manner, we obtain  $B(u) \approx 0$ , and thus  $\bar{f}(u) = \text{const.}$  The deviations from this result as seen in Fig. 12 are due to higher-order phase correlations.

We conclude that, in the portion of the phase space in which no islands appear, the evolution of the velocity distribution can be described by a Fokker-Planck equation. In order to calculate diffusion and frictional coefficients the time step must be chosen to correspond to a sufficiently large number of "collisions" so that the phases are randomized.

*Note added in proof.* A recent article by A. Brahic [Astron. Astrophys. 12, 98 (1971)] deals with some aspects of Fermi acceleration considered in this present article.

#### ACKNOWLEDGMENT

The authors wish to express their thanks to Dr. A. B. Langdon for a number of helpful conversations they have had with him during the course of this work.

\*Work supported in part by the Air Force Office of Scientific Research under Grant No. AFOSR-69-1754 and the National Science Foundation under Grant No. GK-2978.

<sup>1</sup>G. H. Walker and J. Ford, Phys. Rev. 188, 416 (1969).

<sup>2</sup>J. Ford and G. H. Lunsford, Phys. Rev. A 1, 59 (1970).

<sup>3</sup>B. V. Chirikov, E. Keil, and A. M. Sessler, J. Statistical Phys. (to be published).

<sup>4</sup>E. F. Jaeger and A. J. Lichtenberg, Ann. Phys. (N. Y.) (to be published); Bull. Am. Phys. Soc. 14, 1074 (1969).

<sup>5</sup>E. Fermi, Phys. Rev. 75, 1169 (1949).

<sup>6</sup>S. Ulam, in *Proceedings of the Fourth Berkeley Symposium on Mathematics, Statistics, and Probability*

(California U.P., Berkeley, 1961), Vol. 3, p. 315.

<sup>7</sup>J. M. Hammersley, in Ref. 6, Vol. 3, p. 79.

<sup>8</sup>G. M. Zaslavskii and B. V. Chirikov, Dokl. Akad. Nauk SSSR 159, 306 (1964) [Sov. Phys. Doklady 9, 989 (1965)].

<sup>9</sup>J. M. Greene, J. Math. Phys. 9, 760 (1968).

<sup>10</sup>M. Seidl, Plasma Phys. 6, 597 (1964).

<sup>11</sup>J. J. Stoker, *Nonlinear Vibrations in Mechanical and Electrical Systems* (Interscience, New York, 1950), Chap. 3.

<sup>12</sup>V. I. Arnol'd, Russian Math. Surveys 18, 9 (1963).

<sup>13</sup>J. Moser, Nachr. Akad. Wiss. Göttingen, II Math.-Physik, Kl. 1 (1962).

<sup>14</sup>M. C. Wang and G. E. Uhlenbeck, Rev. Mod. Phys. 17, 323 (1945).